Article

Thermoelectric Properties of Layered $CuCr_{0.99}Ln_{0.01}S_2$ (Ln = La...Lu) Disulfides: Effects of Lanthanide Doping

Evgeniy V. Korotaev [ORCID] and Mikhail M. Syrokvashin *

Nikolaev Institute of Inorganic Chemistry, Siberian Branch, Russian Academy of Sciences, 630090 Novosibirsk, Russia
* Correspondence: syrokvashin@niic.nsc.ru

Abstract: A comprehensive study of the thermoelectric properties of $CuCr_{0.99}Ln_{0.01}S_2$ (Ln = La...Lu) disulfides was carried out in a temperature range of 300 to 740 K. The temperature dependencies of the Seebeck coefficient, electrical resistivity, and thermal conductivity were analyzed. It was found that the cationic substitution of chromium with lanthanides in the crystal structure of layered copper–chromium disulfide, $CuCrS_2$ resulted in notable changes in the thermoelectric performance of $CuCr_{0.99}Ln_{0.01}S_2$. The cationic substitution led to an increase in the Seebeck coefficient and electrical resistivity and a thermal conductivity decrease. The highest values of the thermoelectric figure of merit and power factor corresponded to the praseodymium-doped sample and an initial $CuCrS_2$-matrix at 700–740 K. The cationic substitution with lanthanum, cerium, praseodymium, samarium, and terbium allowed for an enhancement of the thermoelectric performance of the initial matrix at a temperature range below 600 K. The cationic substitution of $CuCrS_2$ with lanthanum and praseodymium ions appeared to be the most promising approach for increasing the thermoelectric performance of the initial matrix.

Keywords: layered copper–chromium disulfide; lanthanides; thermoelectricity; Seebeck coefficient; electrical resistivity; thermoelectric figure of merit; power factor

1. Introduction

The layered copper–chromium disulfide $CuCrS_2$ is considered a multipurpose functional material with a quasilayered structure formed by CrS_2-layers separated by a van der Waals gap filled with copper ions [1–8]. Some of the crystallographic sites in this gap are unfilled at room temperature [9–11]. However, under specific conditions, the copper ions are able to hop between these sites, thereby moving throughout the otherwise solid crystal. This phenomenon leads to the order-to-disorder phase transition (ODT) in $CuCrS_2$ disulfide at temperatures above 670 K [10–12]. The presence of the ODT in the high-temperature range in $CuCrS_2$-based compounds results in ferroelectric properties. Thus, these compounds could be considered functional materials for the fabrication of various high-temperature electronic devices, such as tunable ferroelectric capacitors (varactors) and resistors (memristors). The ionic conductivity of $CuCrS_2$-based compounds allows one to consider them promising materials for the fabrication of chemical current sources and chemotronic devices [9,13–18]. The helimagnetic ordering demonstrated at low temperatures by the layered copper–chromium disulfide matrix allows one to consider $CuCrS_2$ a material for the fabrication of solid-state memory devices. The functional properties of $CuCrS_2$-based compounds can be tuned by the cationic substitution of the initial matrix. The cationic substitution of metal atoms in the initial $CuCrS_2$-matrix with V, Mn, or Ag promotes an increase in the ionic conductivity of the prepared compounds [9,13,19,20]. Furthermore, the cationic substitution can induce the emergence of new functional properties in $CuCrS_2$-based compounds. For instance, cationic substitution with V not only enhances the ionic conductivity of $CuCr_{1-x}V_xS_2$ compounds but also induces colossal magnetoresistivity

and metal-to-insulator (MIT) phase transition [21–25]. The substitution of S atoms with Se has been reported to improve the thermoelectric properties of $CuCrS_{2-x}Se_x$ compared with $CuCrX_2$ (X = S, Se) matrix compounds [26,27]. In recent years, the thermoelectric properties of $CuCrS_2$ and layered dichalcogenides, such as $ACrX_2$-type (A = Cu, Ag, Au; X = S, Se), have garnered particular interest. The high values of the Seebeck coefficient value and ionic conductivity allow one to consider $ACrX_2$-matix- and $ACrX_2$-based compounds phonon glass–electron crystal (PGEC) materials [1,4,28,29]. However, the majority of the experimental data correspond to initial matrix compounds. For instance, the layered anti-ferromagnet copper–chromium disulfide $CuCrS_2$ demonstrates enhanced values regarding the thermoelectric figure of merit (ZT), up to ~2 [30,31]. The combination of the aforementioned properties allows $CuCrS_2$-based compounds to be considered promising materials for the fabrication of high-performance thermoelectric generators (TEGs). The cationic substitution of the $CuCrS_2$-matrix is significantly affected by the thermoelectric properties of the initial matrix [32–36]. It was previously reported that the cationic substitution of the $CuCrS_2$-matrix with a low concentration of doping atoms could enhance the thermoelectric properties of the initial matrix. For instance, $CuCrS_2$-based compounds doped with iron atoms, such as $CuCr_{1-x}Fe_xS_2$, up to a concentration of x = 0.03, have demonstrated high values of the Seebeck coefficient [32]. Lanthanide chalcogenides are considered promising compounds for designing of efficient thermoelectric materials [37,38]. This is due to the significant contribution of *f*-states in the formation of the electronic structure of these materials [39,40]. Note that the increased localization of electronic density in the band gap region is considered one of the most significant features determining the total Seebeck coefficient value of semiconductor thermoelectric compounds. Note that an increase in the doping atom concentration in $CuCrS_2$-based compounds causes the suppression of the Seebeck coefficient due to the MIT [23,25,32]. Thus, according to previous studies, a concentration of x = 0.01 is considered to be optimal. Note that the cationic substitution of chromium in the $CuCrS_2$-matrix with lanthanide atoms, from lanthanum to lutecium, in $CuCr_{1-x}Ln_xS_2$ has been reported to occur via the isovalent principle with Cr^{3+} to Ln^{3+} [34,35,39,41]. A study of compounds doped with promethium was excluded from this study due to its radioactivity and rarity. Thus, the enhancement of the Seebeck coefficient can be primarily attributed to the contribution of the *f*-states of lanthanides in the reconstruction of electronic structure resulting from the cationic substitution process. The present study involved experimental data concerning the analysis of the total set of thermoelectric parameters, including electrical resistivity, thermal conductivity, thermoelectric figure of merit (ZT), and power factor (PF), of layered antiferromagnet $CuCr_{0.99}Ln_{0.01}S_2$ (Ln = La...Lu) compounds.

2. Experimental

$CuCr_{0.99}Ln_{0.01}S_2$ (Ln = La...Lu) compounds were synthesized using high-purity commercial metal oxides via the previously reported sulfidation route [34]. The samples were found to be single-phase and isostructural to the initial $CuCrS_2$-matrix [41]. The XRD data evidencing the cationic substitution of the chromium atoms with lanthanides and the study of the doping mechanism were reported previously [35,36,39–41]. The ceramic samples were prepared by compressing the synthesized powder samples under uniaxial pressure in a vacuum [34]. The measurements of the Seebeck coefficient of the $CuCr_{0.99}Ln_{0.01}S_2$ compounds were carried out using the original experimental setup described in detail in [32,34,36].

The electrical resistivity was measured in a rarefied helium atmosphere of 5 Torr using the Van der Pauw technique. Electric probes were fixed on the sample's surface using the conducting compound prepared from a mixture of graphite powder and high-temperature glue. The measurements were carried out using a 6½ Keysight 34465A voltmeter (Keysight Technologies, Santa Rosa, CA, USA). During the measurements, the current direction was reversed. The temperature of the sample was maintained using a Thermodat-13 K5 temperature controller.

The thermal conductivity was studied using a comparative steady-state measurement technique in a vacuum with a residual pressure of 10^{-2} Torr. A quartz disk with a diameter of 10.5 mm and a thickness of 3.2 mm was used as the reference sample. The average dimensions of the ceramic samples of $CuCr_{0.99}Ln_{0.01}S_2$ were the same as those of the reference sample's dimensions. The ceramic sample, the copper disk, and the reference sample were placed between a temperature-controlled copper heater and a heat sink. The temperature in the measurement cell was measured by a thermocouple mounted in a copper disk sandwiched between the sample and the reference. The surfaces of the disks, perpendicular to the heat flow direction, were treated with a mixture of graphite powder and polymethylsiloxane to reduce the thermal contact resistance. The measurement cell volume was surrounded by a brass thermal shield with a temperature three degrees lower than the temperature of the heat sink. A temperature gradient of five degrees between the heater and the heat sink was maintained using a Thermodat-13 K5 temperature controller.

The Hall mobility (μ) for the $CuCr_{0.99}Ln_{0.01}S_2$ compounds was calculated using the values of the electrical resistivity (ρ) at 300 K and charge carrier concentrations (n) reported previously [34] as $\mu = (e \cdot n \cdot \rho)^{-1}$, where e is the elementary charge.

The thermoelectric figure of merit (ZT) was calculated using the measured values of the Seebeck coefficient (S), electrical resistivity (ρ), and thermal conductivity (k) as $ZT = S^2 T/(\rho \cdot k)$. The power factor was calculated as $PF = S^2/\rho$.

3. Results and Discussion

The Seebeck coefficient temperature dependencies S(T) for the initial $CuCrS_2$-matrix and $CuCr_{0.99}Ln_{0.01}S_2$ (Ln = La...Lu) compounds are plotted in Figure 1. The measured S(T) dependencies demonstrated similar behavior to those of the initial matrix. However, the dependency of the compound doped with lanthanum atoms demonstrated a different behavior (red curve in Figure 1). As can be seen in Figure 1, the measured S(T) dependencies can be divided into two regions. The first one corresponds to a temperature range of 300 to 500 K. Here, the doped compounds exhibited an increase in the Seebeck coefficient value compared with the initial matrix, except for the samples doped with Tm and Ce. At the second temperature range (T > 500 K), the compounds doped with La, Ce, Pr, Gd, and Tb demonstrated further increases in the Seebeck coefficient. In contrast, the cationic substitution with other lanthanide atoms caused Seebeck coefficient suppression. At a temperature region of 650–700 K, an inflection feature was observed. As was previously reported, this could be due to the order-to-disorder (ODT) phase transition that occurs in $CuCrS_2$-based compounds [10–12]. Note that for the initial $CuCrS_2$-matrix, the ODT is accompanied by a significant reconstruction of the electronic structure, leading to the vanishing of the band gap [12]. The inflection feature can be primarily observed for $CuCr_{0.99}La_{0.01}S_2$. For clarity, Figure 1 plots the enlarged region of the S(T) within a temperature range ~100 K below and ~50 K above the ODT at ~690 K.

The observed enhancement of the Seebeck coefficient for $CuCr_{0.99}La_{0.01}S_2$ can be attributed to the reconstruction of the band structure during the cationic substitution process [34,35,39]. For instance, the cationic substitution of Cr^{3+} ions, bearing three unpaired electrons in the 3d-level, by La^{3+} with an empty 4f-level, leads to a decrease in the electronic density in the valence band top region. This results in a shift of the valence band top toward a higher binding energy region, thereby increasing the band gap. Consequently, the total Seebeck coefficient value is increased. Thus, one can conclude that the proposed explanation—in the case of doping with Ce or Pr bearing a lower number of electrons compared with Cr—can also be applied to the interpretation of the observed behavior of the S(T) dependencies. The behavior of the S(T) for other lanthanide ions can be attributed to the features of the localization of the 4f-levels in the band structure of $CuCr_{0.99}La_{0.01}S_2$. For instance, the binding energy of the 4f-levels increases with the lanthanide atomic number. Note that an increase in the substitution concentration causes Seebeck coefficient suppression due to the metal-insulator transition (MIT) [32,33]. An increase in the lanthanide concentration to x = 0.03 results in the presence of an additional $CuLnS_2$ impurity phase

in the composition of $CuCr_{1-x}Ln_xS_2$, as was previously shown for lanthanum [33]. The Seebeck coefficient value increases as a function of the lanthanum concentration up to x = 0.015. However, a further increase in the lanthanum concentration leads to Seebeck coefficient suppression due to the metal-to-insulator transition (MIT).
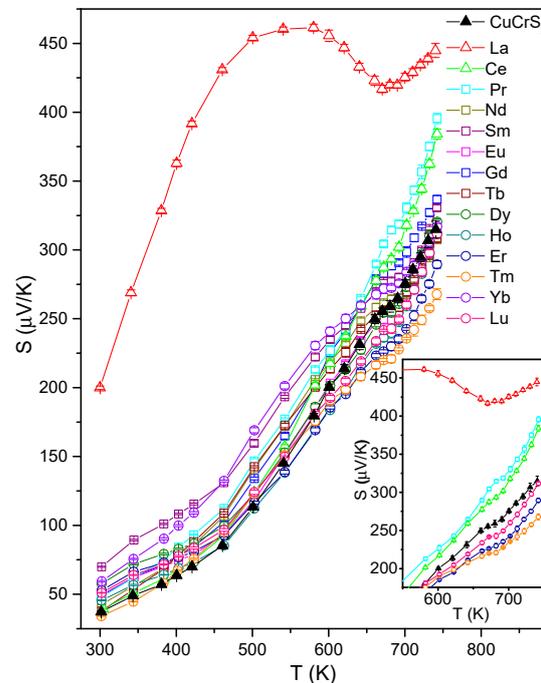

Figure 1. Seebeck coefficient temperature dependencies for initial $CuCrS_2$-matrix and doped $CuCr_{0.99}Ln_{0.01}S_2$ (Ln = La...Lu) disulfides. Inset: The enlarged region of the S(T) within a temperature range ~100 K below and ~50 K above the ODT.
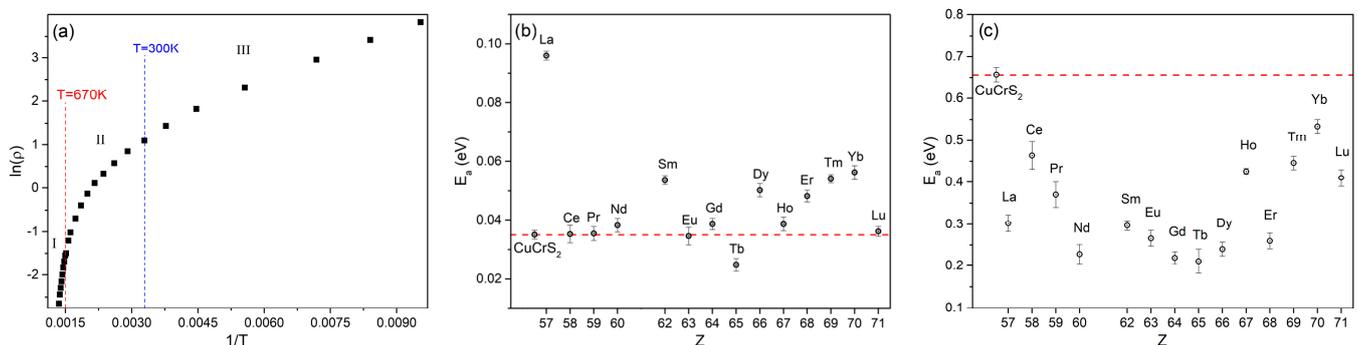
The temperature dependencies of the electrical resistivity (ρ) for $CuCr_{0.99}Ln_{0.01}S_2$ exhibited typical behavior for these semiconductor compounds (Figure 2). The electrical resistivity gradually decreases with temperature. The doped samples, except those with Tb, demonstrate an increase in ρ compared with the initial matrix at 300 K. However, in the high-temperature region, the lower electrical resistivity value corresponds to $CuCrS_2$. In the case of $CuCr_{0.99}Ln_{0.01}S_2$, the lowest value can be observed for $CuCr_{0.99}Pr_{0.01}S_2$, while the largest one can be observed for $CuCr_{0.99}La_{0.01}S_2$.

The representation of $\ln(\rho)$ in the inverse temperature scale (1/T) can be used to estimate the activation energy value (E_a). An example of inverse temperature dependence for the initial $CuCrS_2$-matrix is plotted in Figure 3a. The observed dependence can be divided into several parts, revealing two linear regions. The first one can be attributed to the high-temperature region (T > 670 K), while the second one can be attributed to the lower-temperature region (T < 300 K). The third region between 300 to 670 K exhibited non-linear behavior related to the influence of the ionic conductivity of the $CuCrS_2$-matrix. The calculated values of E_a, as a function of the lanthanide atomic number, are plotted in Figure 3b,c. At temperatures below 300 K, the largest value of E_a corresponds to the La-doped sample, which exhibited the largest values of S (Figure 3b). This could be attributed to the increase in the band gap discussed above. An increase in E_a was also observed in the Sm-, Dy-, Er-, Tm-, and Yb-doped samples. The values of E_a for the samples doped with Ce, Pr, Nd, Eu, and Lu are comparable to those of the initial matrix. The observed decrease in E_a for the Tb-doped sample could be attributed to the localization of the Tb4*f*-states in the energy region between the Fermi level and the conduction band bottom. The linear behavior of $\ln(\rho)$ at the high-temperature range (T > 670 K) is related to a change in the electrical conductivity mechanism of $CuCrS_2$, for instance, the transition from the *p*-type conductivity to mixed electronic–ionic conductivity in $CuCrS_2$-based compounds

at temperatures above 670 K [9,13,14]. The calculated E_a values at T > 670 K are plotted in Figure 3c. Note that the obtained values are one order of magnitude greater compared with those at T < 300 K. The cationic substitution led to a decrease in activation energy compared with the initial matrix. The E_a values tend to decrease up to Tb and then increase. This could be due to an increase in sample defectiveness caused by the difference between the ionic radii of Cr and the substituted ion, as was reported for $CuCr_{1-x}V_xS_2$ [9,13,14].
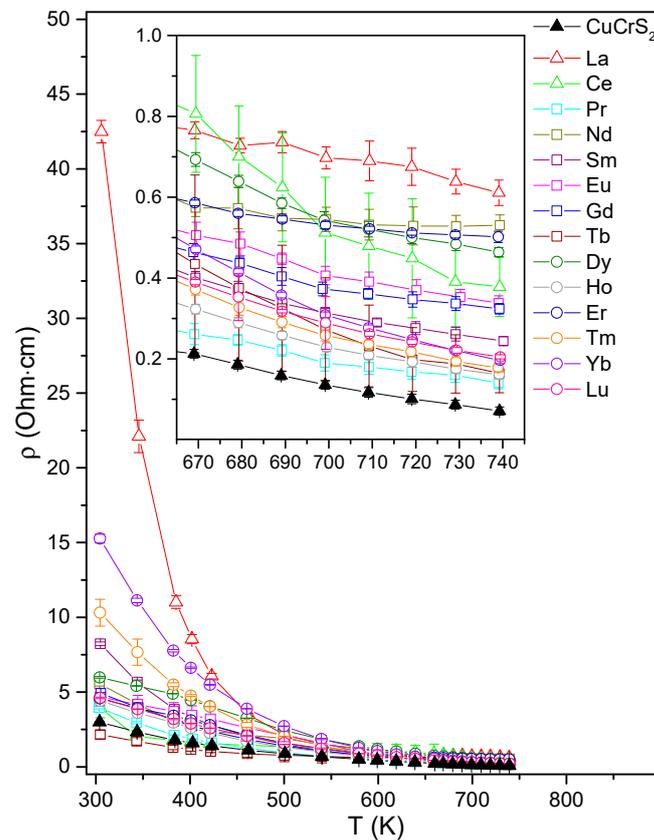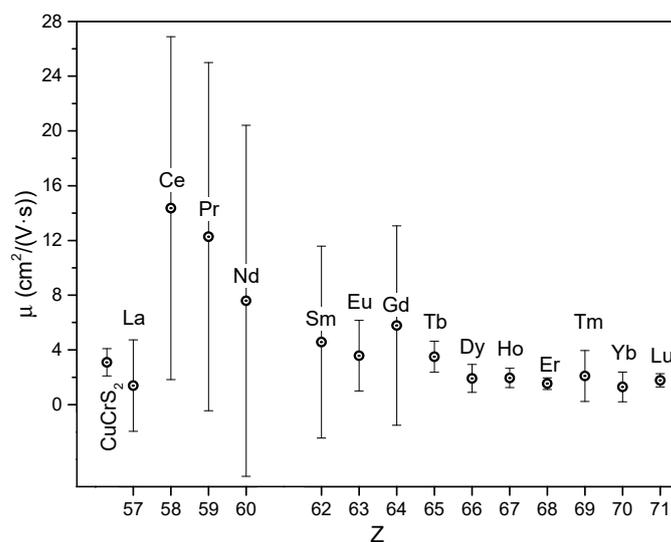

Figure 2. Electrical resistivity temperature dependence for initial $CuCrS_2$-matrix and doped $CuCr_{0.99}Ln_{0.01}S_2$ (Ln = La...Lu) disulfides.

Figure 3. Inverse temperature dependence of electrical resistivity in logarithmic scale for initial $CuCrS_2$-matrix (**a**) and activation energy values for doped $CuCr_{0.99}Ln_{0.01}S_2$ (Ln = La...Lu) disulfides at temperatures below 300 K (**b**) and in a high-temperature range (**c**).

The calculated Hall mobility (μ), as a function of the lanthanide atomic number (Z), is plotted in Figure 4. It was previously shown that the lanthanide atom type affects the charge carrier concentration value. The electronic structure reconfiguration and the redistribution of the partial density of states (pDOS), both in the conduction and in the valence band

during the cationic substitution, result in variation in the charge carrier concentration of $CuCr_{0.99}Ln_{0.01}S_2$. The cationic substitution leads to the emergence of the additional f-states of lanthanide atoms in the Fermi-level region. For instance, the charge carrier concentration value for $CuCr_{0.99}Ln_{0.01}S_2$ doped with lanthanides from La to Gd is decreased compared with the initial $CuCrS_2$-matix [35,39]. Cationic substitution with Tb, Dy, Ho, Er, and Lu demonstrates values comparable to those of the initial $CuCrS_2$-matrix. Thus, one can conclude that the carrier concentration in $CuCr_{0.99}Ln_{0.01}S_2$ is proportional to the lanthanide atomic number. The Hall mobility value, μ, of the initial $CuCrS_2$-matrix was 3 cm^2/(V·s). The obtained value was lower compared with ~10 cm^2/(V·s), which was reported for the crystal flake of $CuCrS_2$ [30]. This could be attributed to the differences in the real spatial structure of the ceramic and crystal flake samples. For instance, the additional scattering of charge carriers at grain boundaries can significantly affect the overall charge carrier mobility. Note that the high confidence intervals for both measured values of the Hall voltage and electrical resistivity resulted in the low accuracy of the final carrier mobility value for the doped samples from La to Gd. However, the tendency of μ to decrease towards the end of the lanthanide series can be observed. This could be attributed to an increase in the scattering of charge carriers by the heavier lanthanide ions. Note that the decrease in charge carrier mobility correlates with an increase in the electrical resistivity of $CuCr_{1-x}Ln_xS_2$ compounds compared with the initial $CuCrS_2$-matrix.

Figure 4. Hall mobility for initial $CuCrS_2$-matrix and doped $CuCr_{0.99}Ln_{0.01}S_2$ (Ln = La...Lu) disulfides at 300 K.

The behavior of the thermal conductivity temperature dependencies for the $CuCrS_2$-matrix and the lanthanide-doped samples was similar (Figure 5). The obtained dependencies can be divided into two regions. The first one corresponds to an increase in thermal conductivity due to an increase in both the charge carrier concentration and the lattice thermal conductivity at 300–500 K. Note that the lattice thermal conductivity is determined by the heat capacity, phonon phase velocity, and phonon mean free path length [42,43]. The heat capacity of $CuCr_{0.99}Ln_{0.01}S_2$ increases as a function of temperature, reaching a maximum of the ODT temperature region [12,41]. The thermal conductivity at the higher temperature range can be attributed to a heat capacity decrease or an increase in the phonon scattering induced by the mobile copper cations (the PGEC concept). The thermal conductivity value of ~1 W/(m·K) measured for the initial $CuCrS_2$-matrix correlated well with the data reported previously [30,31,44,45]. The cationic substitution led to a decrease in the thermal conductivity of $CuCr_{0.99}Ln_{0.01}S_2$ compared with the initial matrix, except for the samples doped with Tb and Lu. This could be attributed to the greater atomic mass of lanthanides compared with chromium, which promotes an increase in phonon scattering.

The observed increase in the Tb- and Lu-doped samples could be due to the increased sample's thermal contact conductance. Note that, unfortunately, the direct separation of the total thermal conductivity for the doped $CuCr_{0.99}Ln_{0.01}S_2$ compounds into electronic and lattice components according to the Wiedemann–Franz law is not possible. This is due to several reasons. Firstly, this principle is limited to degenerate semiconductors and metals. Secondly, the mixed ion–electron type of conductivity in $CuCrS_2$-based compounds is also affected by the total thermal conductivity.
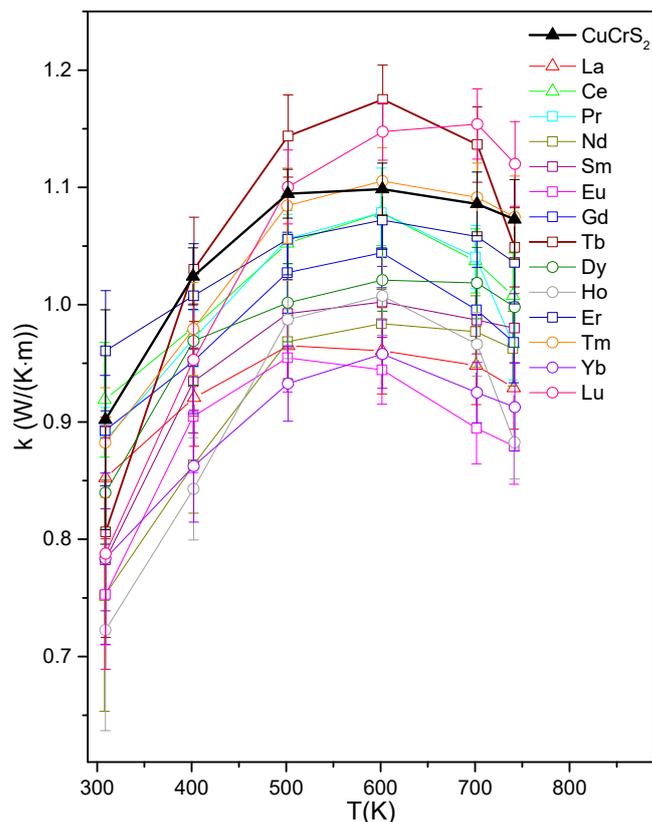
Figure 5. Thermal conductivity temperature dependencies for initial $CuCrS_2$-matrix and doped $CuCr_{0.99}Ln_{0.01}S_2$ (Ln = La...Lu) disulfides.

The temperature dependencies of the thermoelectric figure of merit (ZT) for the doped $CuCr_{0.99}Ln_{0.01}S_2$ (Ln = La...Lu) compounds and the initial $CuCrS_2$-matrix are plotted in Figure 6a. In the room temperature region, both the initial $CuCrS_2$-matrix and $CuCr_{0.99}Ln_{0.01}S_2$ exhibited low ZT values ($\sim 10^{-7} \div 10^{-6}$) owing to the high electrical resistivity of the samples studied. As discussed above, the Seebeck coefficient of $CuCr_{0.99}Ln_{0.01}S_2$ increases with temperature, while the electrical resistivity decreases, resulting in an increase in ZT. The cationic substitutions with La, Ce, Pr, Sm, and Tb allow one to increase the ZT value in a temperature range below 600 K compared with the initial matrix. The most significant enhancement of ZT was observed for the $CuCr_{0.99}La_{0.01}S_2$ sample. The largest ZT value, ~0.09, was obtained for the praseodymium-doped sample and the initial $CuCrS_2$-matrix at 740 K. Thus, La and Pr can be considered the most promising lanthanides for enhancing the thermoelectric properties of the initial $CuCrS_2$-matrix. Another important parameter of thermoelectric materials is the power factor (PF). The initial matrix and Ln-doped samples exhibited a low PF of $\sim 10^{-6}$ mW/(m·K^2) at temperatures below 500 K. The largest PF, ~0.14 mW/(m·K^2), corresponded to the initial $CuCrS_2$-matrix at 740 K. The samples doped with La and Pr exhibited a similar trend to that observed for ZT, suggesting that they are the most promising lanthanides for enhancing the power factor (PF) of the initial $CuCrS_2$-matrix.
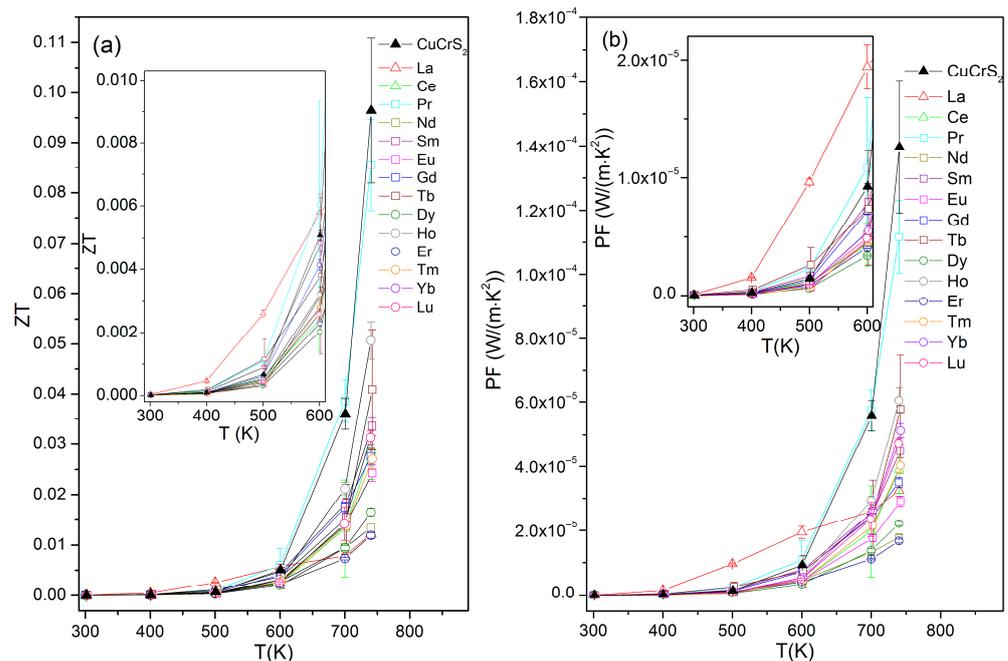
Figure 6. Thermoelectric figure of merit (**a**) and power factor (**b**) temperature dependencies for initial $CuCrS_2$-matrix and doped $CuCr_{0.99}Ln_{0.01}S_2$ (Ln = La. . .Lu) disulfides.

The obtained value of ZT for the initial $CuCrS_2$-matrix is consistent with data reported in [45] and much lower than the values reported in [30,31]. Note that the value of ZT is significantly affected by the synthesis route [31,44]. The most significant parameter affecting the value of ZT is electrical resistivity [31,42,43]. Therefore, reducing the material electrical resistivity could be a means of further enhancing both the ZT and PF parameters of $CuCrS_2$-based compounds. The enhanced thermoelectric performance and low electrical resistivity of the samples doped with La and Pr allow one to consider these compounds promising materials for the design of composite materials. The increased values of ZT at high temperatures allow one to expect further enhancement of the thermoelectric performance of $CuCrS_2$-based materials at T > 740 K.

4. Conclusions

A comprehensive study of all thermoelectric parameters, including the Seebeck coefficient, electrical resistivity, thermal conductivity, the thermoelectric figure of merit, and power factor, was carried out for lanthanide-doped $CuCr_{0.99}Ln_{0.01}S_2$ (Ln = La. . .Lu) disulfides. The cationic substitution of chromium atoms in $CuCrS_2$ with lanthanides affected the thermoelectric properties of the initial matrix. The most significant enhancement of the Seebeck coefficient was observed for the La-doped sample. Cationic substitution allows one to increase both the ZT and PF values of samples doped with La, Ce, Pr, Sm, and Tb at a temperature range below 600 K. The most significant enhancement of ZT was observed for $CuCr_{0.99}La_{0.01}S_2$. The largest value of ZT, ~0.09, was obtained for $CuCr_{0.99}Pr_{0.01}S_2$ at 740 K. The order-to-disorder phase transition (ODT) at T~670 K significantly affected the thermoelectric parameters of $CuCr_{0.99}Ln_{0.01}S_2$. The enhanced thermoelectric performance and low electrical resistivity of the samples doped with La and Pr allow one to consider these compounds promising materials for the design of composite materials. The increased values of ZT at high temperatures allow one to expect further enhancement of the thermoelectric performance of $CuCrS_2$-based materials at T > 740 K. The high value of the Seebeck coefficient makes doped $CuCr_{0.99}Ln_{0.01}S_2$ disulfides promising functional materials for the fabrication of high-temperature sensors.

Author Contributions: Conceptualization, E.V.K. and M.M.S.; methodology, E.V.K.; software, E.V.K.; validation, E.V.K. and M.M.S.; formal analysis, E.V.K. and M.M.S.; investigation, E.V.K.; resources,

References

1. Ushakov, A.V.; Kukusta, D.A.; Yaresko, A.N.; Khomskii, D.I. Magnetism of Layered Chromium Sulfides MCrS2 (M=Li, Na, K, Ag, and Au): A First-Principles Study. *Phys. Rev. B—Condens. Matter Mater. Phys.* **2013**, *87*, 014418. [CrossRef]
2. Engelsman, F.M.R.; Wiegers, G.A.; Jellinek, F.; Van Laar, B. Crystal Structures and Magnetic Structures of Some Metal(I) Chromium(III) Sulfides and Selenides. *J. Solid State Chem.* **1973**, *6*, 574–582. [CrossRef]
3. Karmakar, A.; Dey, K.; Chatterjee, S.; Majumdar, S.; Giri, S. Spin Correlated Dielectric Memory and Rejuvenation in Multiferroic CuCrS$_2$. *Appl. Phys. Lett.* **2014**, *104*, 052906. [CrossRef]
4. Hansen, A.-L.; Dankwort, T.; Groß, H.; Etter, M.; König, J.; Duppel, V.; Kienle, L.; Bensch, W. Structural Properties of the Thermoelectric Material CuCrS$_2$ and of Deintercalated Cu$_x$CrS$_2$ on Different Length Scales: X-ray Diffraction, Pair Distribution Function and Transmission Electron Microscopy Studies. *J. Mater. Chem. C* **2017**, *5*, 9331–9338. [CrossRef]
5. Lee, H.K.; Ban, Y.J.; Lee, H.J.; Kim, J.H.; Park, S.J. One-Pot Synthesis and Characterization of CuCrS$_2$/ZnS Core/Shell Quantum Dots as New Blue-Emitting Sources. *Materials* **2023**, *16*, 762. [CrossRef]
6. Sanchez Rodriguez, J.J.; Nunez Leon, A.N.; Abbasi, J.; Shinde, P.S.; Fedin, I.; Gupta, A. Colloidal Synthesis, Characterization, and Photoconductivity of Quasi-Layered CuCrS$_2$ Nanosheets. *Nanomaterials* **2022**, *12*, 4164. [CrossRef] [PubMed]
7. Xu, X.; Zhong, T.; Zuo, N.; Li, Z.; Li, D.; Pi, L.; Chen, P.; Wu, M.; Zhai, T.; Zhou, X. High-T_C Two-Dimensional Ferroelectric CuCrS$_2$ Grown via Chemical Vapor Deposition. *ACS Nano* **2022**, *16*, 8141–8149. [CrossRef] [PubMed]
8. Zhong, T.; Li, X.; Wu, M.; Liu, J.M. Room-Temperature Multiferroicity and Diversified Magnetoelectric Couplings in 2D Materials. *Natl. Sci. Rev.* **2020**, *7*, 373–380. [CrossRef]
9. Al'mukhametov, R.F.; Yakshibaev, R.A.; Gabitov, É.V.; Abdullin, A.R. Investigation of Superionic Phase Transition in the CuCr$_{1−x}$V$_x$S$_2$ System by X-Ray Diffraction and Magnetic Methods. *Phys. Solid State* **2000**, *42*, 1508–1511. [CrossRef]
10. Vassilieva, I.G.; Kardash, T.Y.; Malakhov, V.V. Phase Transformations of CuCrS$_2$: Structural and Chemical Study. *J. Struct. Chem.* **2009**, *50*, 288–295. [CrossRef]
11. Vasilyeva, I.G. Chemical Aspect of the Structural Disorder in CuCrS$_2$ and CuCr$_{1−x}$V$_x$S$_2$ Solid Solutions. *J. Struct. Chem.* **2017**, *58*, 1009–1017. [CrossRef]
12. Korotaev, E.V.; Syrokvashin, M.M.; Filatova, I.Y.; Sotnikov, A. V Effect of the Order-Disorder Transition on the Electronic Structure and Physical Properties of Layered CuCrS$_2$. *Materials* **2021**, *14*, 2729. [CrossRef] [PubMed]
13. Al'mukhametov, R.F.; Yakshibaev, R.A.; Gabitov, E.V.; Abdullin, A.R. Synthesis and X-Ray Diffraction Study of CuCr$_{1−x}$V$_x$S$_2$. *Inorg. Mater.* **2000**, *36*, 437–440. [CrossRef]
14. Almukhametov, R.F.; Yakshibayev, R.A.; Gabitov, E.V.; Abdullin, A.R.; Kutusheva, R.M. Structural Properties and Ionic Conductivities of CuCr$_{1−x}$V$_x$S$_2$ Solid Solutions. *Phys. Status Solidi Basic Res.* **2003**, *236*, 29–33. [CrossRef]
15. Titov, S.V.; Gorbenko, A.P.; Yakshibaev, R.A.; Reznichenko, L.A.; Al'mukhametov, R.F.; Titov, V.V.; Shilkina, L.A. Ion Conductivity, Structural Features, and Multifractal Properties of Grain Boundaries in CuCr$_{1−x}$V$_x$S$_2$. *Bull. Russ. Acad. Sci. Phys.* **2007**, *71*, 719–720. [CrossRef]
16. Almukhametov, R.F.; Yakshibaev, R.A.; Kutusheva, R.M.; Amineva, A. Structural Properties and Ionic Conductivity of New CuCr$_{1−x}$V$_x$Se$_2$ Solid Solutions. *Solid State Ion.* **2003**, *158*, 409–414. [CrossRef]
17. Yakshibaev, R.A.; Akmanova, G.R.; Almukhametov, R.F.; Konev, V.N. Ionic Conductivity and Diffusion in CuCrS$_2$—AgCrS$_2$ Mixed Conductors and Their Alloys. *Phys. Status Solidi* **1991**, *124*, 417–426. [CrossRef]
18. Krengel, M.; Hansen, A.L.; Hartmann, F.; van Dinter, J.; Bensch, W. Elucidation of the Sodium—Copper Extrusion Mechanism in CuCrS$_2$: A High Capacity, Long-Life Anode Material for Sodium-Ion Batteries. *Batter. Supercaps* **2018**, *1*, 176–183. [CrossRef]
19. Akmanova, G.R.; Davletshina, A.D. Ionic Conductivity and Diffusion in Superionic Conductors CuCrS$_2$—AgCrS$_2$. *Lett. Mater.* **2013**, *3*, 76–78. [CrossRef]

20. Al'mukhametov, R.F.; Yakshibaev, R.A.; Abdullin, A.R. Preparation and Magnetic Properties of $CuCr_{1-X}Mn_XS_2$ Solid Solutions. *Inorg. Mater.* **2002**, *38*, 447–449. [CrossRef]

21. Abramova, G.M.; Petrakovskiǐ, G.A.; Vorotynov, A.M.; Velikanov, D.A.; Kiselev, N.I.; Bovina, A.F.; Szymczak, R.; Al'mukhametov, R.F. Phase Transitions and Colossal Magnetoresistance in $CuV_xCr_{1-x}S_2$ Layered Disulfides. *JETP Lett.* **2006**, *83*, 118–121. [CrossRef]

22. Abramova, G.M.; Petrakovskiǐ, G.A.; Vtyurin, A.N.; Vorotynov, A.M.; Velikanov, D.A.; Krylov, A.S.; Gerasimova, Y.; Sokolov, V.V.; Bovina, A.F. Magnetic Properties, Magnetoresistance, and Raman Spectra of $CuV_xCr_{1-x}S_2$. *Phys. Solid State* **2009**, *51*, 532–536. [CrossRef]

23. Abramova, G.M.; Petrakovskii, G.A. Metal-Insulator Transition, Magnetoresistance, and Magnetic Properties of 3d-Sulfides. *Low Temp. Phys.* **2006**, *32*, 725–734. [CrossRef]

24. Abramova, G.M.; Vorotynov, A.M.; Petrakovskiǐ, G.A.; Kiselev, N.I.; Velikanov, D.A.; Bovina, A.F.; Al'Mukhametov, R.F.; Yakshibaev, R.A.; Gabitov, É.V. Electron Transition in Intercalated Disulfide $CuCrS_2$. *Phys. Solid State* **2004**, *46*, 2225–2228. [CrossRef]

25. Tsujii, N.; Kitazawa, H.; Kido, G. Insulator to Metal Transition Induced by Substitution in the Nearly Two-Dimensional Compound $CuCr_{1-X}V_xS_2$. *Phys. Status Solidi* **2006**, *3*, 2775–2778. [CrossRef]

26. Romanenko, A.I.; Chebanova, G.E.; Katamanin, I.N.; Drozhzhin, M.V.; Artemkina, S.B.; Han, M.-K.; Kim, S.-J.; Wang, H. Enhanced Thermoelectric Properties of Polycrystalline $CuCrS_{2-x}Se_X$ (x = 0, 0.5, 1.0, 1.5, 2) Samples by Replacing Chalcogens and Sintering. *J. Phys. D. Appl. Phys.* **2021**, *55*, 135302. [CrossRef]

27. Srivastava, D.; Tewari, G.C.; Karppinen, M.; Nieminen, R.M. First-Principles Study of Layered Antiferromagnetic $CuCrX_2$ (X = S, Se and Te). *J. Phys. Condens. Matter* **2013**, *25*, 105504. [CrossRef] [PubMed]

28. Wu, D.; Huang, S.; Feng, D.; Li, B.; Chen, Y.; Zhang, J.; He, J. Revisiting $AgCrSe_2$ as a Promising Thermoelectric Material. *Phys. Chem. Chem. Phys.* **2016**, *18*, 23872–23878. [CrossRef]

29. Bhattacharya, S.; Basu, R.; Bhatt, R.; Pitale, S.; Singh, A.; Aswal, D.K.; Gupta, S.K.; Navaneethan, M.; Hayakawa, Y. $CuCrSe_2$: A High Performance Phonon Glass and Electron Crystal Thermoelectric Material. *J. Mater. Chem. A* **2013**, *1*, 11289–11294. [CrossRef]

30. Tewari, G.C.; Tripathi, T.S.; Kumar, P.; Rastogi, A.K.; Pasha, S.K.; Gupta, G. Increase in the Thermoelectric Efficiency of the Disordered Phase of Layered Antiferromagnetic $CuCrS_2$. *J. Electron. Mater.* **2011**, *40*, 2368–2373. [CrossRef]

31. Tewari, G.C.; Tripathi, T.S.; Rastogi, A.K. Thermoelectric Properties of Layer-Antiferromagnet $CuCrS_2$. *J. Electron. Mater.* **2010**, *39*, 1133–1139. [CrossRef]

32. Korotaev, E.V.; Syrokvashin, M.M.; Filatova, I.Y.; Pelmenev, K.G.; Zvereva, V.V.; Peregudova, N.N. Seebeck Coefficient of Cation-Substituted Disulfides $CuCr_{1-x}Fe_xS_2$ and $Cu_{1-x}Fe_xCrS_2$. *J. Electron. Mater.* **2018**, *47*, 3392–3397. [CrossRef]

33. Korotaev, E.V.; Syrokvashin, M.M.; Filatova, I.Y. Thermoelectric and Magnetic Properties and Electronic Structure of Solid Solutions $CuCr_{1-x}La_xS_2$. *J. Compos. Sci.* **2023**, *7*, 436. [CrossRef]

34. Korotaev, E.V.; Syrokvashin, M.M.; Filatova, I.Y.; Sotnikov, A.V.; Kalinkin, A.V. The Charge Distribution, Seebeck Coefficient, and Carrier Concentration of $CuCr_{0.99}Ln_{0.01}S_2$ (Ln = Dy–Lu). *Materials* **2023**, *16*, 2431. [CrossRef] [PubMed]

35. Korotaev, E.V.; Syrokvashin, M.M.; Filatova, I.Y.; Sotnikov, A.V.; Kalinkin, A.V. Charge Distribution in Layered Lanthanide-Doped $CuCr_{0.99}Ln_{0.01}S_2$ (Ln = Pr–Tb) Thermoelectric Materials. *Materials* **2022**, *15*, 8747. [CrossRef] [PubMed]

36. Korotaev, E.V.; Syrokvashin, M.M.; Filatova, I.Y.; Trubina, S.V.; Nikolenko, A.D.; Ivlyushkin, D.V.; Zavertkin, P.S.; Sotnikov, A.V.; Kriventsov, V.V. XANES Investigation of Novel Lanthanide-Doped $CuCr_{0.99}Ln_{0.01}S_2$ (Ln = La, Ce) Solid Solutions. *Appl. Phys. A Mater. Sci. Process.* **2020**, *126*, 537. [CrossRef]

37. Dmitriev, A.V.; Zvyagin, I.P. Current Trends in the Physics of Thermoelectric Materials. *Uspekhi Fiz. Nauk.* **2010**, *180*, 821. [CrossRef]

38. Shevelkov, A.V.; Шевельков, А.В. Chemical Aspects of the Design of Thermoelectric Materials. *Russ. Chem. Rev.* **2008**, *77*, 1–19. [CrossRef]

39. Korotaev, E.V.; Syrokvashin, M.M.; Filatova, I.Y.; Kalinkin, A.V.; Sotnikov, A.V. Valence Band Structure and Charge Distribution in the Layered Lanthanide-Doped $CuCr_{0.99}Ln_{0.01}S_2$ (Ln = La, Ce) Solid Solutions. *Sci. Rep.* **2021**, *11*, 18934. [CrossRef]

40. Korotaev, E.V.; Syrokvashin, M.M.; Filatova, I.Y.; Trubina, S.V.; Nikolenko, A.D.; Ivlyushkin, D.V.; Zavertkin, P.S.; Kriventsov, V.V. The Conduction Band of the Lanthanide Doped Chromium Disulfides $CuCr_{0.99}Ln_{0.01}S_2$ (Ln=La, Ce, Gd): XANES Investigations. In *AIP Conference Proceedings, Proceedings of the Synchrotron and Free Electron Laser Radiation: Generation and Application (SFR-2020), Novosibirsk, Russia, 13–16 July 2020*; AIP Publishing: New York, NY, USA, 2020; Volume 2299, p. 080004.

41. Korotaev, E.V.; Syrokvashin, M.M.; Filatova, I.Y.; Zvereva, V.V. Magnetic Properties of Novel Layered Disulfides $CuCr_{0.99}Ln_{0.01}S_2$ (Ln = La...Lu). *Materials* **2021**, *14*, 5101. [CrossRef]

42. Terasaki, I. Thermal Conductivity and Thermoelectric Power of Semiconductors. In *Reference Module in Materials Science and Materials Engineering*; Elsevier: Amsterdam, The Netherlands, 2016; pp. 1–40. ISBN 9780128035818.

43. Aswal, D.K.; Basu, R.; Singh, A. Key Issues in Development of Thermoelectric Power Generators: High Figure-of-Merit Materials and Their Highly Conducting Interfaces with Metallic Interconnects. *Energy Convers. Manag.* **2016**, *114*, 50–67. [CrossRef]

44. Kaltzoglou, A.; Vaqueiro, P.; Barbier, T.; Guilmeau, E.; Powell, A.V. Ordered-Defect Sulfides as Thermoelectric Materials. *J. Electron. Mater.* **2014**, *43*, 2029–2034. [CrossRef]

45. Chen, Y.-X.; Zhang, B.-P.; Ge, Z.-H.; Shang, P.-P. Preparation and Thermoelectric Properties of Ternary Superionic Conductor CuCrS$_2$. *J. Solid State Chem.* **2012**, *186*, 109–115. [CrossRef]